Analysis of Model Parameters Affecting the Pressure Profile in a Circulating Fluidized Bed

Sofiane Benyahia
National Energy Technology Laboratory, Morgantown, WV 26507

DOI 10.1002/aic.12603
Published online March 31, 2011 in Wiley Online Library (wileyonlinelibrary.com).

This study focuses on continuum model validation of the flow of air and small catalyst particles in a circulating fluidized bed. Comparison with available experimental data of pressure drop and solids circulation rate in the riser clearly demonstrates the need to modify the homogeneous drag model to accurately predict the formation of clusters of particles, which are typically observed in the fluidization of small particles. The need to correct the drag law is also demonstrated in simulations of polydisperse powder flows wherein three solids species are used to represent a typical catalyst size distribution. Finally, particle-wall friction is found to have the most significant effect on the vertical gas pressure gradient while particle–particle friction has only a minor effect. Published 2011 American Institute of Chemical Engineers *AIChE J*, 58: 427–439, 2012
Keywords: circulation fluidized beds, computational fluid dynamics (CFD), fluidization, multiphase flow, particulate flows

Introduction

Flows of particles are commonly encountered in nature, such as in volcanic ash eruptions and dust storms, and in most industries, such as in chemical and energy conversion technologies. Complex flow phenomena observed in these particulate flows are attributed to particle–particle and particle-fluid interactions that are difficult to model with a high degree of accuracy. Although accurate, direct numerical simulations (DNS) of these flow phenomena are only possible for small-scale idealized systems due to current limitations in computational resources.[1] A more economical approach is to use averaged fluid flow equations solved on a coarse computational domain and to track the motion of each individual particle following Newton's law of motion with necessary closures for particle-fluid interaction forces. Note the tracking of particles and their collisions is possible even for millions of particles.[2] However, such simulations become very difficult to conduct for those industrial systems where the flow rate of particles is measured in tons per second.[3] An even more computationally economical approach can be derived from the averaged continuum equations of motion for both the fluid and particles, which is often called the two-fluid model.[4] The continuum approach generally relies on closures for the solids stresses that are derived from granular kinetic theory[5] in the kinetic-collisional regime and from soil mechanics in the dense-frictional regime.[6]

Most modeling efforts for fluidized systems are conducted using the continuum or two-fluid model simply because of the limited computer resources currently available. Moreover, for these continuum simulations to be conducted fast enough to be useful they are routinely used with coarse computational grids. The simulation predictions resulting from using coarse grids may not be accurate because a grid-size as small as a few particles in diameters was shown to be necessary for the prediction of bed height expansion of small Geldart A catalyst particles in a bubbling fluidized bed.[7] Thus, continuum simulations of large-scale gas-solids processes with appropriate grid resolution are made impractical. Similarly, an earlier work by Agrawal et al.[8] has shown that grid-refined two-fluid flow simulations can predict heterogeneous structures that cannot be captured with coarse-grid simulations using the same model. Agrawal et al.[8] found that the formation of clusters of

Correspondence concerning this article should be addressed to S. Benyahia at sofiane.Benyahia@netl.doe.gov.

particles reroute the flow of gas around them effectively increasing the slip velocity by more than twice the homogeneous settling velocity of particles. Therefore, any coarse grid continuum simulation of gas-solids flow must include subgrid corrections to the homogeneous drag force acting on the particles. Benyahia[9] studied gas-solids flow in a dense riser and found that subgrid corrections to the homogeneous drag force are both essential and useful to accurately predict the radial profiles of solids density and mass flux.

Li and Kwauk[10] proposed the energy-minimization multiscale (EMMS) model to account for the effects of the heterogeneous structures on the drag force. In the EMMS model, the structures in circulating fluidized beds were characterized with the dense cluster phase and the dilute phase. The parameters related to the dense and the dilute phases were determined by satisfying a stability condition, namely $N_{st} \rightarrow \min$, where N_{st} denotes the mass-specific energy consumption for suspending and transporting particles (W/kg). The subgrid correction to the homogeneous drag force based on the EMMS model[11,12] was found necessary to accurately predict the axial profile of the solids density.

As mentioned earlier, several studies published in the open literature have demonstrated the need to include subgrid corrections for two-fluid models. This study indicates that similar corrections are also required for the continuum modeling of gas and polydisperse powders (sometimes called multifluid models) in a circulating fluidized bed. In particular, an EMMS model is shown to accurately predict the solids circulation rate and gas pressure gradient in the fully-developed flow region. However, the numerical results of pressure gradient profiles in the mid-bottom section of the riser are under-predicted and require further investigation. The work presented in this paper also found that the generally accepted assumption that the gas pressure gradient is balanced by the weight of the bed is inaccurate as a large portion of solids accumulates in the annulus region and falls under gravity and is, thus, not supported by the gas pressure. Further efforts conducted in this study include the effects of particle–particle and particle-wall friction on the vertical profiles of solids hold-up and pressure gradient.

Gas-Solids Flow Model

The continuum governing equations, constitutive relations, and boundary conditions for the flow of a monodisperse powder in air are described in Table 1. The gas phase is described via averaged equations of motion, specifically, the single-phase continuum Navier-Stokes equations for a Newtonian fluid, modified to include the fluid volume fraction as well as the fluid-particle interaction due to the drag force. A constant gas viscosity is used through most of the flow domain except in very dilute regions where a constant mixing-length model is adopted (Eq. 9). The primary purpose of using this mixing-length model is to avoid strong vortices that develop early (during the initial filling with solids) in the simulation and cause convergence problems. A detailed description of the different mixing-length models can be found in the book by Pope.[14] The use of a laminar gas viscosity in most of the flow domain is motivated by the study of Benyahia et al.[15] who showed that, under moderately dense flow conditions, the gas-phase turbulent stresses could be neglected without any noticeable effect on the time-averaged flow profiles.

The monodisperse granular kinetic theory developed by Lun et al.[16] modified to include the effects of the interstitial fluid by Balzer et al.[17] and Lun and Savage[18] is used in most of this study. The only exception is the polydisperse case where a discrete particle size distribution of three solids species is used. The polydisperse case is modeled using a kinetic theory developed by Iddir and Arastoopour[19] with some modifications described by Benyahia.[20] A detailed description of this polydisperse model is beyond the scope of this study and interested readers are referred to the dissertations of Iddir[21] and Galvin[22] for details of the derivation of this theory and its numerical implementation.

In flow regions approaching the random packing of particles where enduring contacts between particles occur, the granular kinetic theories mentioned earlier are not valid due to the assumptions used in their derivation, namely instantaneous binary collisions. In these dense flow regions, the frictional theory developed by Srivastava and Sundaresan[23] provides a frictional pressure and viscosity that are added to the stresses derived from granular kinetic theory. This frictional flow theory was validated by other studies in the literature.[24,25] The frictional-collisional wall boundary conditions (Eqs. 22 and 23) derived by Johnson and Jackson[26] are used in all simulations.

One of the most important forces in a fluidized system is due to fluid-particle drag and, therefore, the predictive accuracy of the multiphase flow model will depend on the accuracy of this constitutive model. In this study, the well-known Wen-Yu drag correlation is used, which was derived empirically for homogeneous flows and is commonly adopted in fluidization literature (see for example, Gidaspow[5]). The Wen-Yu drag function can be modified to account for the heterogeneous flow structures commonly observed in the fluidization of small particles by air such as in the visual observations of clusters of particles forming in a fluidized bed that were reported by Cocco et al.[27] Such corrections to this standard drag law are available in the literature.[12,28] This effort employs the correction by Lu et al.,[12] which is based on the energy minimization and multiscale (EMMS) theory. A detailed description of this model and its derivation was presented by Lu et al.[12] and is not repeated here for the sake of brevity. The numerical predictions, obtained with and without this correction factor (Eq. 7), are compared to experimental data to demonstrate the necessity of accounting for the presence of particle clusters.

Simulation Conditions

The simulated riser geometry, physical properties of gas and fluid catalytic cracking catalyst (FCC), as well as flow conditions are the same as those used in the simulations by Lu et al.[12] The riser has a height of 10.5 m and width of 0.09 m with a 2D Cartesian geometry. Unlike Lu et al.[12] who considered initial conditions of a static bed close to packing, the initial static bed height is set to $\sim$ 2.78 m corresponding to minimum fluidization conditions ($\varepsilon_s^{mf} = 0.4$). The initial mass of solids is the same as that used by Lu et al.[12] The mass of solids in the bed is constant throughout the current simulations since the solids exiting the top of the

Table 1. Gas-solids Hydrodynamic Model

Governing equations

Conservation of mass for phase m (s: solids and g: gas):

$$\frac{\partial(\rho_{\mathrm{m}}\varepsilon_{\mathrm{m}})}{\partial t}+\nabla\cdot(\rho_{\mathrm{m}}\varepsilon_{\mathrm{m}}\mathbf{v}_{\mathrm{m}})=0 \tag{1}$$

Conservation of linear momentum:

$$\left[\frac{\partial(\rho_{\mathrm{m}}\varepsilon_{\mathrm{m}}\mathbf{v}_{\mathrm{m}})}{\partial t}+\nabla\cdot(\rho_{\mathrm{m}}\varepsilon_{\mathrm{m}}\mathbf{v}_{\mathrm{m}}\mathbf{v}_{\mathrm{m}})\right]=-\varepsilon_{\mathrm{m}}\nabla P_{\mathrm{g}}+\nabla\cdot(\tau_{\mathrm{m}})-\beta_{\mathrm{m}n}(\mathbf{v}_{\mathrm{m}}-\mathbf{v}_{n})+\varepsilon_{\mathrm{m}}\rho_{\mathrm{m}}\mathbf{g} \tag{2}$$

Translational granular energy conservation equation:

$$\frac{3}{2}\rho_{\mathrm{s}}\left[\frac{\partial(\varepsilon_{\mathrm{s}}\Theta_{\mathrm{s}})}{\partial t}+\nabla\cdot(\varepsilon_{\mathrm{s}}\Theta_{\mathrm{s}}\mathbf{v}_{\mathrm{s}})\right]=-\nabla\cdot\mathbf{q}+\tau_{\mathrm{c}}\mathbf{:}\nabla\mathbf{v}_{\mathrm{s}}-J_{\mathrm{s}}+\Pi_{\Theta} \tag{3}$$

Interphase momentum exchange term ($\beta_{\mathrm{gs}}=\beta_{\mathrm{sg}}=\beta$):

Wen-Yu correlation:

$$\beta=\frac{3}{4}C_{\mathrm{D}}\frac{\rho_{\mathrm{g}}\varepsilon_{\mathrm{g}}\varepsilon_{\mathrm{s}}\left|\mathbf{v}_{\mathrm{g}}-\mathbf{v}_{\mathrm{s}}\right|}{d_{\mathrm{p}}}\varepsilon_{\mathrm{g}}^{-2.65} \tag{4}$$

$$C_{\mathrm{D}}=\begin{cases}24/Re\left(1+0.15Re^{0.687}\right) & Re<1000\\ 0.44 & Re>1000\end{cases},Re=\frac{\rho_{\mathrm{g}}\varepsilon_{\mathrm{g}}\left|\mathbf{v}_{\mathrm{g}}-\mathbf{v}_{\mathrm{s}}\right|d_{\mathrm{p}}}{\mu_{\mathrm{g}}} \tag{5}$$

EMMS drag model:

$$\beta=\begin{cases}150\frac{\varepsilon_{\mathrm{s}}\left(1-\varepsilon_{\mathrm{g}}\right)\mu_{\mathrm{g}}}{\varepsilon_{\mathrm{g}}d_{\mathrm{p}}^{2}}+1.75\frac{\rho_{\mathrm{g}}}{d_{\mathrm{p}}}\varepsilon_{\mathrm{s}}\left|\mathbf{v}_{\mathrm{g}}-\mathbf{v}_{\mathrm{s}}\right| & \varepsilon_{\mathrm{g}}<0.4\\ \frac{3}{4}C_{\mathrm{D}}\frac{\rho_{\mathrm{g}}\varepsilon_{\mathrm{g}}\varepsilon_{\mathrm{s}}\left|\mathbf{v}_{\mathrm{g}}-\mathbf{v}_{\mathrm{s}}\right|}{d_{\mathrm{p}}}\varepsilon_{\mathrm{g}}^{-2.65}H_{\mathrm{d}} & \varepsilon_{\mathrm{g}}\geq 0.4\end{cases} \tag{6}$$

$$H_{\mathrm{d}}=A_{\mathrm{e}}(Re+B_{\mathrm{e}})^{C_{\mathrm{e}}} \tag{7}$$

$$\varepsilon_{\mathrm{g}}\geq 0.9997\begin{cases}A_{\mathrm{e}}=1\\ B_{\mathrm{e}}=1\\ C_{\mathrm{e}}=0\end{cases}$$

$$\varepsilon_{\mathrm{g}}\geq 0.99\begin{cases}A_{\mathrm{e}}=0.4243+0.88/\left(1+e^{\frac{(0.9942-\varepsilon_{\mathrm{g}})}{2.18\times10^{-3}}}\right)\left(1-1/\left(1+e^{\frac{(0.9989-\varepsilon_{\mathrm{g}})}{3\times10^{-5}}}\right)\right)\\ B_{\mathrm{e}}=1.661\times10^{-2}+0.2436e^{-0.5\left(\frac{(0.9985-\varepsilon_{\mathrm{g}})}{1.91\times10^{-3}}\right)^{2}}\\ C_{\mathrm{e}}=8.25\times10^{-2}-0.0574e^{-0.5\left(\frac{(0.9979-\varepsilon_{\mathrm{g}})}{7.03\times10^{-3}}\right)^{2}}\end{cases}$$

$$\varepsilon_{\mathrm{g}}\geq 0.545\begin{cases}A_{\mathrm{e}}=\left(49.1698-49.5722\,\varepsilon_{\mathrm{g}}\right)^{-0.4896}\\ B_{\mathrm{e}}=\left(137.6308-21.6308\,\varepsilon_{\mathrm{g}}\right)^{13.031}\\ C_{\mathrm{e}}=\dfrac{\varepsilon_{\mathrm{g}}-1.0013}{-6.633\times10^{-2}+9.1391(\varepsilon_{\mathrm{g}}-1.0013)+6.9231(\varepsilon_{\mathrm{g}}-1.0013)^{2}}\end{cases}$$

(*Continued*)

$$\varepsilon_g \geq 0.46 \begin{cases} A_e = 3.2 \times 10^{-2} + \dfrac{0.7399}{1 + (\varepsilon_g/0.4912)^{54.4265}} \\ B_e = 2.25 \times 10^{-3} + \dfrac{772.0074}{1 + 10^{66.3224(\varepsilon_g - 0.3987)}} + \dfrac{2.404 \times 10^{-2}}{1 + 10^{53.8948(0.5257 - \varepsilon_g)}} \\ C_e = 0.1705 - \dfrac{0.1731}{1 + (\varepsilon_g/0.5020)^{37.7091}} \end{cases}$$

$$\varepsilon_g \geq 0.4 \begin{cases} A_e = 0.8526 - \dfrac{0.5846}{1 + (\varepsilon_g/0.4325)^{22.6279}} \\ B_e = 1 \\ C_e = 0 \end{cases}$$

Constitutive relations for gas and solids phases

Gas-phase stress tensor:

$$\tau_g = 2\mu_t \mathbf{S}_g \tag{8}$$

$$\mu_t = \begin{cases} \mu_g & \varepsilon_g \leq 0.999 \\ \mu_g + \rho_g l_{mix}^2 \sqrt{2S_g : S_g} & \varepsilon_g > 0.999 \end{cases} \tag{9}$$

$$\mathbf{S}_m = \frac{1}{2}\left(\nabla \mathbf{v}_m + (\nabla \mathbf{v}_m)^T\right) - \frac{1}{3}\nabla \cdot \mathbf{v}_m \mathbf{I} \tag{10}$$

Solids-phase stress tensor:

$$\tau_s = [-(P_s + P_f) + \eta\mu_b \nabla \cdot \mathbf{v_s}]\mathbf{I} + 2(\mu_s + \mu_f)\mathbf{S_s} \tag{11}$$

Solids kinetic-collisional pressure:

$$P_s = \varepsilon_s \rho_s \Theta_s [1 + 4\eta \varepsilon_s g_0] \tag{12}$$

The radial distribution function at contact:

$$g_0 = \frac{1 - 0.5\varepsilon_s}{(1 - \varepsilon_s)^3} \tag{13}$$

Solids viscosity model:

$$\mu_s = \left(\frac{2 + \alpha}{3}\right)\left[\frac{\mu^*}{g_0 \eta (2 - \eta)}\left(1 + \frac{8}{5}\eta \varepsilon_s g_0\right)\left(1 + \frac{8}{5}\eta(3\eta - 2)\varepsilon_s g_0\right) + \frac{3}{5}\eta\mu_b\right] \tag{14}$$

$$\mu^* = \mu\left[1 + \frac{2\beta\mu}{(\varepsilon_s \rho_s)^2 g_0 \Theta_s}\right]^{-1}, \mu = \frac{5}{96}\rho_s d_p \sqrt{\pi\Theta_s}, \mu_b = \frac{256}{5\pi}\mu\varepsilon_s^2 g_0 \tag{15}$$

Granular energy flux and conductivity:

$$\mathbf{q} = -\kappa_s \nabla \Theta_s \tag{16}$$

(*Continued*)

$$\kappa_s = \left(\frac{\kappa^*}{g_0}\right)\left[\left(1+\frac{12}{5}\eta\varepsilon_s g_0\right)\left(1+\frac{12}{5}\eta^2(4\eta-3)\varepsilon_s g_0\right)+\frac{64}{25\pi}(41-33\eta)\eta^2(\varepsilon_s g_0)^2\right] \tag{17}$$

$$\kappa^* = \kappa\left[1+\frac{6\beta\kappa}{5(\varepsilon_s\rho_s)^2 g_0\Theta_s}\right]^{-1}, \kappa = \frac{75\rho_s d_p\sqrt{\pi\Theta_s}}{48\eta(41-33\eta)} \tag{18}$$

Frictional solids pressure and viscosity:

$$\frac{P_f}{P_c} = \left(1-\frac{\nabla\cdot\mathbf{v_s}}{n\sqrt{2}\sin(\delta)\sqrt{\mathbf{S_s}:\mathbf{S_s}+\Theta_s/d_p^2}}\right)^{n-1}, \mu_f = \frac{\sin(\delta)}{\sqrt{2}}\frac{P_f}{\sqrt{\mathbf{S_s}:\mathbf{S_s}+\Theta_s/d_p^2}}\left\{n-(n-1)\left(\frac{P_f}{P_c}\right)^{\frac{1}{n-1}}\right\} \tag{19}$$

$$\text{Where, } P_c = \begin{cases} 10^{25}\left(\varepsilon_s-\varepsilon_s^{max}\right)^{10} & \varepsilon_s > \varepsilon_s^{max} \\ Fr\dfrac{\left(\varepsilon_s-\varepsilon_s^{min}\right)^r}{\left(\varepsilon_s^{max}-\varepsilon_s\right)^s} & \varepsilon_s^{max} \geq \varepsilon_s > \varepsilon_s^{min} \\ 0 & \varepsilon_s \leq \varepsilon_s^{min} \end{cases} \text{ and } n = \begin{cases} \frac{\sqrt{3}}{2}\sin(\delta) & \nabla\cdot\mathbf{v_s} \geq 0 \\ 1.03 & \nabla\cdot\mathbf{v_s} < 0 \end{cases} \tag{20}$$

Collisional dissipation of granular energy and viscous damping terms:

$$J_s = \frac{48}{\sqrt{\pi}}\eta(1-\eta)\frac{\rho_s\varepsilon_s^2 g_0}{d_p}\Theta_s^{3/2}, \Pi_\Theta = -3\beta\Theta_s + 81\frac{\varepsilon_s\mu_g^2\left|\mathbf{v_g}-\mathbf{v_s}\right|^2}{g_0 d_p^3\rho_s\sqrt{\pi\Theta_s}} \tag{21}$$

Gas-solids wall boundary conditions

Gas-phase: free slip.

Solids phase: Johnson-Jackson partial slip[26]

$$\frac{\mathbf{v_{sl}}}{|\mathbf{v_{sl}}|}\cdot(\tau_k+\tau_f)\cdot\mathbf{n}+\frac{\phi\pi\rho_s\varepsilon_s g_0\sqrt{\Theta_s}}{2\sqrt{3}\varepsilon_s^{max}}\mathbf{v_{sl}}+(\mathbf{n}\cdot\tau_f\cdot\mathbf{n})\tan\delta_w = 0 \tag{22}$$

$$\mathbf{n}\cdot\mathbf{q} = \frac{\phi\pi|\mathbf{v_{sl}}|^2\rho_s\varepsilon_s g_0\sqrt{\Theta_s}}{2\sqrt{3}\varepsilon_s^{max}} - \frac{\sqrt{3}\pi\rho_s\varepsilon_s g_0\left(1-e_w^2\right)\sqrt{\Theta_s}}{4\varepsilon_s^{max}}\Theta_s \tag{23}$$

riser via two pressure outlets re-enter near the bottom via two inlets with $\varepsilon_s^{in} = 0.3$. The solids velocity at the two inlets is automatically adjusted to achieve the same flow rate of solids exiting the system. See Figure 1 for more clarity on the geometry and initial and boundary conditions.

Table 2 shows the physical parameters used in this current effort. The majority of the simulations are monodisperse with FCC particles of the Group A (aeratable) Geldart classification of powder. These particles are not highly cohesive and, from a modeling point of view, it seems possible to ignore cohesive forces and obtain good agreement with experimental data as long as the computational mesh is fine enough.[7] The carrier gas is air at isothermal and ambient conditions. Two physical properties, the particle–particle restitution coefficient and the particle-wall specularity coefficient, are varied to study their effects. Two simulations of FCC particles with a particle size distribution (PSD) consisting of three solids species are also conducted in this study. Table 3 shows the PSD in the initial static bed, which was taken from Kunii and Levenspiel[13] (p. 66), who considered it as "typical." Thus, the continuous PSD is discretized into three bins, each with an averaged particle size and volume fraction (or mass fraction since the solids density is the same for all particle sizes). A better approach would be to adopt the size distribution of the experimental FCC particles, but such information was not available. Nevertheless, this study qualitatively demonstrates the effect of PSD on the vertical pressure drop and size-segregation of particles.

The MFIX CFD code (https://mfix.netl.doe.gov) is used to discretize the governing equations with the finite volume

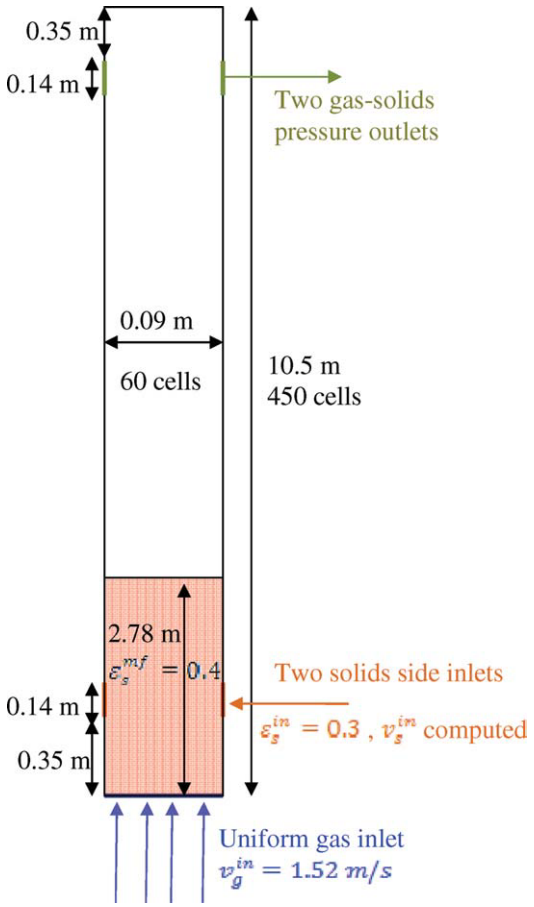

Figure 1. Schematic drawing of 2D riser geometry (not to scale) with boundary and initial conditions.

The 60 by 450 computational grid points are uniformly distributed along the riser width and height, respectively.

technique and solves these equations on a staggered grid. All equations were discretized using the Superbee second-order scheme along with deferred correction.[29] The transient numerical solution is obtained within a residual tolerance of less than 10^{-3} for all equations but the granular energy equation, which has a residual tolerance less than 10^{-4}. Note that the residual for the pressure correction equation (modified continuity equation) is scaled using the first iteration

Table 2. Gas and Solids Physical Parameters

Process temperature	297 K
Process pressure	1.01×10^5 Pa
Air density	Computed using ideal gas law (about 1.2 kg/m^3)
Air viscosity	1.8×10^{-5} Pa·s
Gas-phase turbulence length-scale	0.01 m
Solids density	930 kg/m^3
Particle diameter	54 μm
Single-particle terminal velocity	0.074 m/s
Particle–particle restitution coefficient	0.9
Particle-wall restitution coefficient	0.7
Specularity coefficient	0.0001
Particle-particle angle of friction	$\pi/6$
Particle-wall angle of friction	$\pi/16$
Void fraction at maximum packing	0.4
Void fraction at minimum fluidization	0.6

Table 3. Particle Size Distribution for the Polydisperse Cases

Solids species	d_{p30}	d_{p60}	d_{p115}
Particle diameter (μm)	30	60	115
Volume or mass fraction (%)	15	60	25

residual at each time-step. A variable time-stepping procedure in MFIX guarantees convergence at each time-step, or the failed time-step will be reduced until a converged solution is achieved. An averaged time-step of about 10^{-4} sec is necessary for the monodisperse simulations, and a slightly lower time-step is necessary for polydisperse simulations. The relatively low time-step used in these simulations is due to the fact that the numerical implementation of the flow model is semi-implicit. For polydisperse flows, more terms are treated explicitly and, therefore, a lower time-step is necessary to run these simulations. A typical simulation requires 8 hours for monodisperse case and 4 days for polydisperse case (with three solids species) of CPU time per second of transient flow time on a shared memory machine using two processors. An optimum grid density of 60 by 450, previously found by Lu et al.,[12] is adopted in all our simulations.

Results and Discussion

The computed instantaneous values of the dimensionless drag correlations (Hd) used in the EMMS model (see Eq. 7) are shown in Figure 2. Hd is defined as the ratio of the subgrid drag coefficient over that obtained using the Wen-Yu drag law at the same conditions. Values of Hd = 1 are plotted for the Wen-Yu correlation to illustrate that the EMMS model predicts values of Hd less than unity over a wide range of void fractions. The lower values predicted by the EMMS drag correlation have been linked to higher solids hold-up for gas solids-flows in risers by Benyahia[9] and are responsible for the formation of large clusters of particles, which is demonstrated later in this effort. Also, as expected from Eq. 7, Hd depends not only on void fraction but also on the *Re* number. Such dependence on void fraction has been plotted by Lu et al.[12] and shows a wider scatter of the data compared with the data plotted in Figure 2. Therefore,

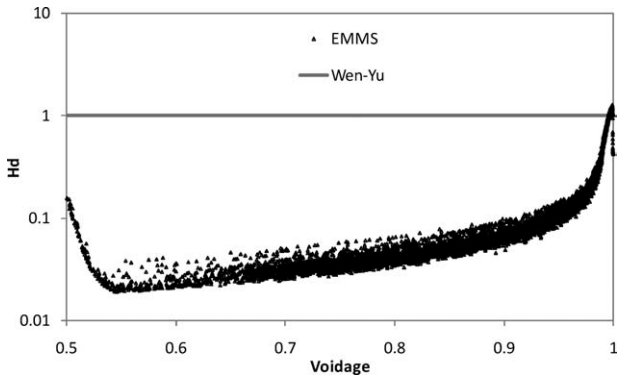

Figure 2. Variation with void fraction of the instantaneous (after 40 sec) dimensionless drag index (H_d) obtained with the EMMS technique during the fluidized bed simulation. The Wen-Yu drag index is just a constant equal to one.

Figure 3. Instantaneous (after 15 sec) and time-averaged (15–40 sec) solids volume fraction contour profiles in the 2D riser geometry (not to scale) where blue, green, yellow and red indicate dilute (near 0%), moderately dilute (about 14%), moderately dense (about 21%) and dense (30% and higher) flow regions, respectively.

[Color figure can be viewed in the online issue, which is available at wileyonlinelibrary.com.]

the simulations of this fluidized bed are characterized by a relatively narrow range of particles' *Re* number due to the fact that the slip velocity does not vary much throughout the system. In other words, large values of *Re* number are theoretically possible, but are not predicted for the small FCC particles used in this study.

Figure 3 shows the instantaneous (after 15 sec of simulation) and time-averaged (from 15 to 40 sec) solids volume fraction profiles in the 2D fluidized bed. In the instantaneous plots, the Wen-Yu drag correlation predicts a fairly homogeneous flow throughout the riser, similar to the previous findings of Lu et al.[12] In contrast, dense heterogeneous structures (clusters of particles) are apparent with the EMMS drag model. These large clusters of particles are observed in the bottom and mid-section of the riser and mainly near the wall regions, while the top region of the riser is generally more dilute. The fact that the solids density (or hold-up) decreases with height is typical of fluidized beds and has been well documented experimentally.[13] In the time-averaged plots, core-annulus flow in the bottom and mid-section of the riser becomes apparent when using the EMMS drag model. The core-annulus regime is represented by regions of dense flow near the walls and relatively dilute flow regions at the core of the riser in the time-averaged results. The only exception is near the two side inlets at the bottom of the riser where the injected solids, recycled from the two top outlets, reach the core regions of the riser. There is a large body of experimental evidence in the literature summarized in fluidization books, such as that of Kunii and Levenspiel[13] and Gidaspow[5] that point to the existence of a core-annulus flow in the fast-fluidization regime and that the solids concentration is higher near the walls where the gas entrainment velocity is lower (as is the case here). Therefore, the evidence derived from experimental measurements already tends to favor the results obtained using the EMMS model over the Wen-Yu drag model, at least qualitatively. The next step is to quantitatively verify this observation.

Figure 4 shows the transient behavior of solids mass flux exiting the system through the two top outlets. For both drag models used in these simulations, a little more than 5 sec are needed for the solids to fill the riser. The Wen-Yu drag model shows large spikes in the solids mass flux after 5 sec, which indicate that a large amount of solids exited the system at that time. In other words, a large section of the bed was initially transported to the top of the riser. This behavior does not occur with the EMMS model due to the computed large clusters of particles (see Figure 3) that fall under their own weight, and thus minimize the amount of solids reaching the top outlets. Note that the solids mass flux data predicted with the Wen-Yu drag law are about an order of magnitude higher than results obtained with EMMS drag model. As a result, different vertical scales were needed to represent these data in Figure 4. After about 15 sec of simulation, both simulations reach a statistically steady-state where data can be collected and used for time-averaging.

Table 4 provides the time-averaged solids mass flux and the standard deviation corresponding to the data plotted in Figure 4. The EMMS drag model predicts the measured solids mass flux reasonably well, but the Wen-Yu drag model

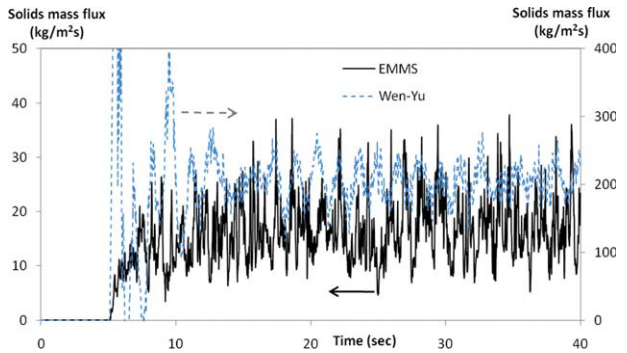

Figure 4. Transient behavior of total solids mass flux through the two outlets located near the top of the riser.

Data related to the Wen-Yu and the EMMS drag models should be read on the right and left vertical axis, respectively. [Color figure can be viewed in the online issue, which is available at wileyonlinelibrary.com.]

Table 4. Solids Mass Flux Predicted at Outlet of Riser for Two Drag Correlations

Drag model	Wen-Yu	EMMS	Experimental
Solids mass flux (kg/m^2s)	205	16.9	14.3
Standard deviation (kg/m^2s)	25.2	5.59	–

predicts a value an order of magnitude larger. This comparison clearly demonstrates the need of subgrid drag modeling to accurately predict gas-solids riser flows in the absence of appropriate grid resolution. Although the EMMS drag model slightly overpredicts the solids mass flux, it is in good agreement with the simulation predictions of Lu et al.[12] in which the same drag model was used. Table 4 also shows the standard deviation of the transient solids mass flux. When scaled with the mean flux, the fluctuations of solids mass flux predicted with the Wen-Yu drag model are lower than those predicted with the EMMS model. This difference can also be seen in Figure 4.

Figure 5 presents a comparison of the predicted time-averaged (15–40 sec) and spatially averaged (along the width of the bed) gas volume fraction (also called void fraction or voidage) and experimental data measured along the height of the riser. The solids hold-up, or the void fraction along the riser height, is usually obtained one of two ways: by direct measurements of void fraction or by deducing the void fraction from pressure drop measurements. The latter approach assumes that the measured gas pressure gradient equals the weight of the bed. An analytical expression of void fraction as function of pressure gradient can be obtained from the steady-state mixture momentum equation (obtained by summing Eq. 2 in Table 1 over the gas and solids phases), and by neglecting inertia and stresses: $\varepsilon_g = \left\{\rho_s + \left(\mathbf{1}/_g \frac{\partial \boldsymbol{P}_g}{\partial y}\right)\right\} \Big/ (\rho_s - \rho_g)$, where the pressure gradient $(\frac{\partial \boldsymbol{P}_g}{\partial y})$ has negative values. In this equation, similar results for void fraction can be obtained if the total weight of the bed is considered to consist only of solids, due to the high density of the solids material. Note that in Figure 5 the experimental measurement for the void fraction is indirectly deduced from pressure drop measurements (labeled pressure) while the simulation predictions for void fraction are calculated using both techniques with those using the direct method labeled ''voidage'' and those using the indirect method labeled ''pressure.''

Comparing the experimental measurement for the void fraction to that computed directly from the EMMS model shows good agreement in the lower section of the bed and a slight underprediction at the upper section of the riser. In contrast, the void fraction computed directly from the Wen-Yu drag model significantly underpredicts the experimental data at the upper section of the riser, indicating that in the real system large amount of solids are not transported to the top section of the riser. The computed void fraction data using the EMMS model also agrees reasonably well with the simulation predictions by Lu et al.,[12] in which the same drag model and grid density (60 by 450) are used.

The experimental void fraction data is also compared with the simulation prediction for voidage obtained indirectly from the gradient of gas pressure. Thus, the value of the pressure gradient can be inferred from the shown voidage profile, and an overprediction in voidage indicates an underprediction in pressure gradient and vice versa. As evident from Figure 5, the values of pressure gradient corresponding to the Wen-Yu drag model are consistently larger than the experimental data in the fully-developed flow region (upper region of the riser). On the other hand, the EMMS drag model accurately predicts the pressure gradient (again expressed in term of void fraction) in the upper region above 5 m. However, the EMMS drag model clearly underpredicts the pressure drop in the mid-bottom section of the riser even though the computed void fraction using this model agreed reasonably well. Figure 5 clearly shows for the case of the EMMS model that the computed solids hold-up is larger than the computed pressure gradient throughout the height of the riser. The fact that the gas pressure gradient does not balance the weight of the bed is an indication that solids (and gas) must flow downward in a region located near the walls for the case of a core-annulus flow regime. This reasoning is clearly demonstrated in the radial profiles of solids density and flux, which are presented next.

Before proceeding, however, one final point in regard to the large differences between the computed voidage and pressure gradient profiles shown in Figure 5 is worth discussing. This variation indicates, at least for this case, that the assumption that the gas pressure gradient approximately balances the weight of the bed (commonly used to represent experimental data) may not be accurate along much of the height of the bed, especially in regions where large

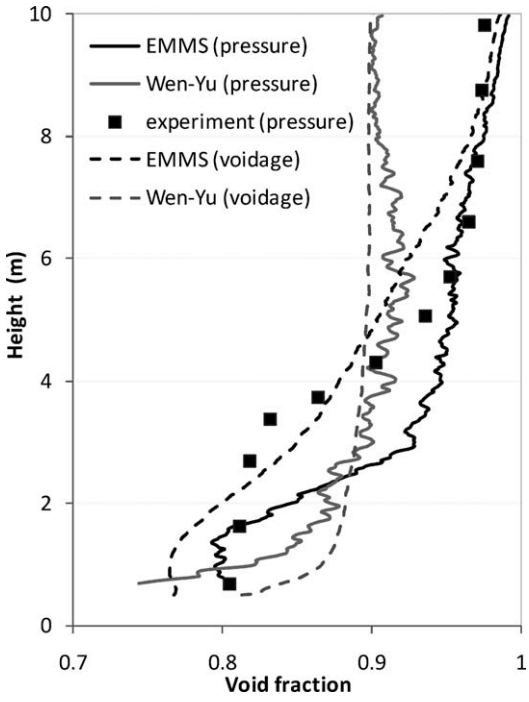

Figure 5. Time-averaged void fraction along the height of the riser computed with the drag models used in this study.

The void fraction is plotted using either the computed void fraction (shown as voidage) or deduced from computed pressure gradients (shown as pressure) while the experimental void fraction was deduced from pressure drop measurements. Note that experimental errors are not known.

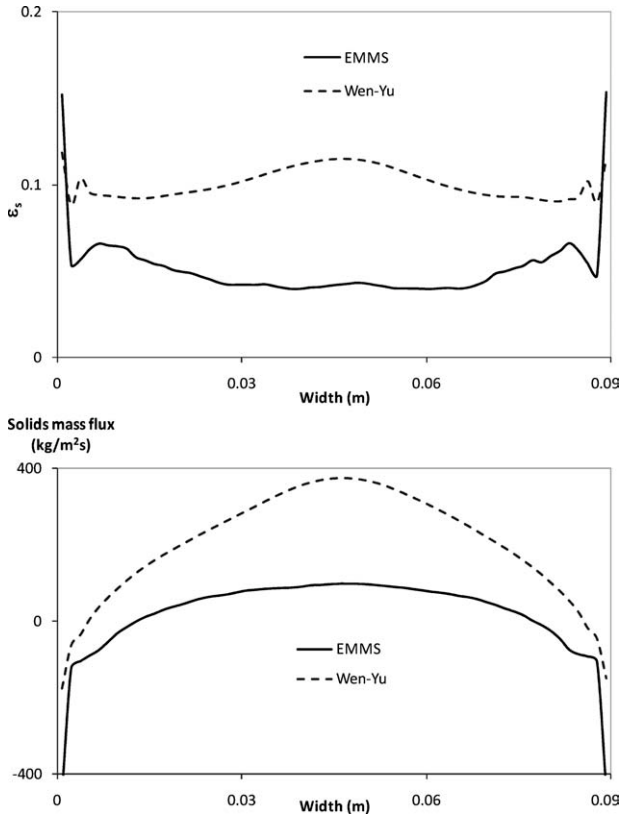

Figure 6. Time-averaged solids volume fraction and mass flux plotted along the width of the riser at a height of 7 m above the gas uniform inlet distributor.

variations of pressure gradients occur. However, this commonly used assumption may be more accurate in the upper, fully developed flow regions in the riser.

Figure 6 presents the time-averaged (15-40 sec) solids volume fraction and mass flux along the width of the riser in the fully-developed flow region at a height of 7 m above the gas uniform distributor. A core-annulus flow regime is clearly shown for the EMMS drag model where the solids concentration is larger at the walls, and more dilute conditions are computed at the core of the riser. This behavior is not apparent for the Wen-Yu drag model where a large concentration of solids is evident in the core region. Solids downflow near the walls of the riser is computed using both drag models, although much larger downward fluxes are computed with the EMMS drag model. The predictions of solids mass flux using the Wen-Yu drag shows much larger upflow at the core and smaller downflow at the annulus as compared with EMMS drag model, which explains the solids hold-up data presented in Figure 5 and the average solids fluxes summarized in Table 4. In particular, the large solids concentration predicted at the core region for the Wen-Yu drag model must be lifted by the gas, which clearly explains the large pressure drop and low void fractions computed at the upper regions of the riser, as shown in Figure 5. In addition, the fact that the EMMS drag model fails to correctly predict the pressure gradient at the mid-bottom section of the riser (from a height of about 2 to 5 m in Figure 5) seems to indicate that either a larger solids hold-up occurs in that region or a more uniform distribution of solids along the width of the riser may be required. This premise is investigated in the following sections.

Effect of particle–particle contact friction

The frictional contact between two rotating particles is not included in the current model, summarized in Table 1, due to additional complexity that arises from solving additional equations. Fortunately, a straightforward correction to the linear particle–particle restitution coefficient was demonstrated by Jenkins and Zhang[30] to show accurate results for slightly frictional particles. By using this simple correction one can avoid solving additional equations for the rotational component of momentum and energy of the particles. The effective coefficient is expressed as: $e' = e - \frac{\pi}{2}\mu + \frac{9}{2}\mu^2$, where only in this specific equation μ is the contact friction coefficient. Similar to previous studies by Jenkins and Zhang[30] and Benyahia[20] μ is assumed equal to 0.1. So a value of $e = 0.9$, taken from Table 2, corresponds to a value of effective coefficient of $e' = 0.79$ and demonstrates that extra dissipation of energy will occur due to frictional contacts between particles, facts that were previously ignored. Therefore, to study the effects of friction requires modifying only the restitution coefficient, and all other properties are kept the same (see Table 2).

The time-averaged results showing the effect of particle–particle friction on the predicted vertical profiles of void

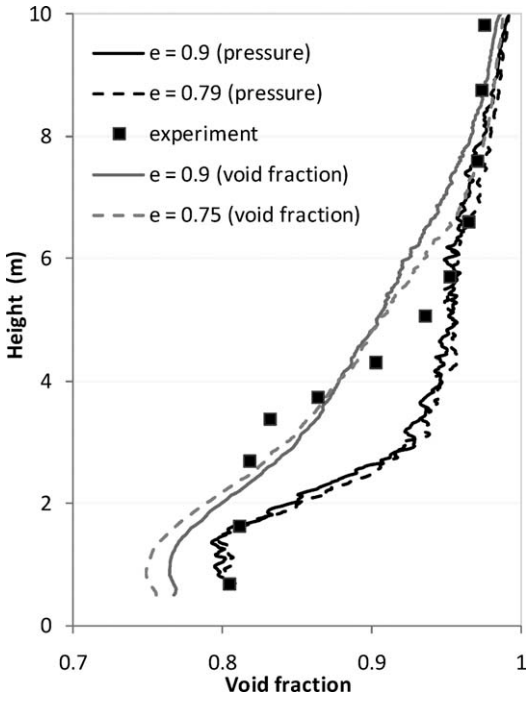

Figure 7. Indirect effect of particle-particle friction (obtained by reducing restitution coefficient) on the vertical profiles of computed void fraction (shown as void fraction) and calculated void fraction deduced from computed pressure gradient (shown as pressure) for the EMMS model.

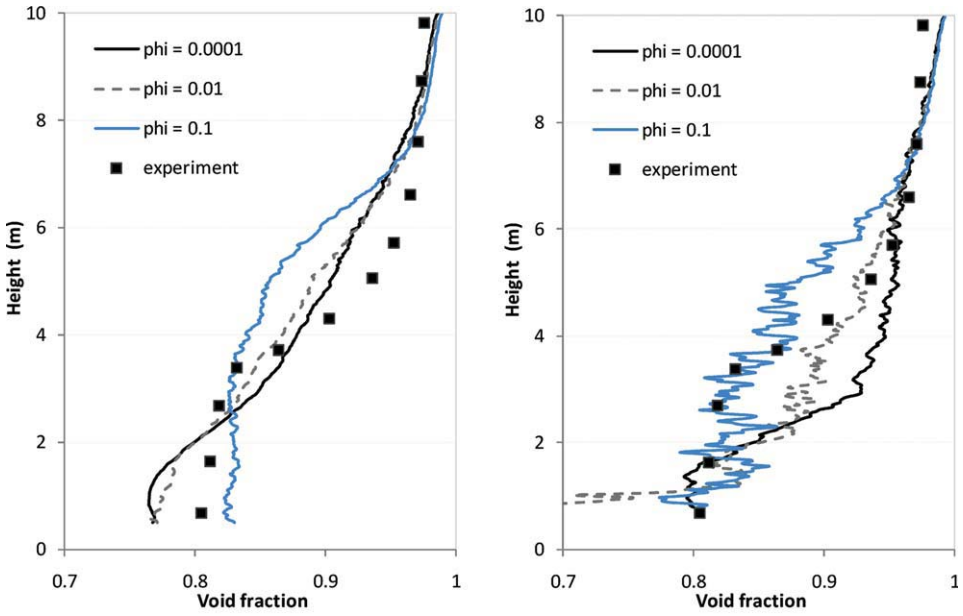

(a) Numerical data based on computed void fraction

(b) Numerical data based on computed pressure gradient

Figure 8. Effect of particle-wall friction (obtained by varying specularity coefficient phi) on the vertical profiles of computed void fraction (shown in the figure on the left) and calculated void fraction deduced from computed pressure gradient (shown in the figure on right) for the EMMS model.

Time-averaged simulation data obtained for three values of phi are compared with pressure-gradient experimental data. [Color figure can be viewed in the online issue, which is available at wileyonlinelibrary.com.]

fraction obtained directly (labeled voidage) and indirectly (labeled pressure; recall the pressure gradient is inferred from this computed voidage profile) are presented in Figure 7 for the EMMS model. Reducing the restitution coefficient had no noticeable effect on the pressure gradient profiles throughout the height of the riser. However, a noticeable deviation on the void fraction (or solids hold-up) profile is observed near the bottom and top regions of the riser. In particular, a larger solids hold-up is noticeable at the bottom region of the riser while a smaller solids hold-up is predicted at the upper region when reducing the restitution coefficient. The fact that the opposite effect on solids hold-up is observed between the bottom and top regions is reasonable because the total inventory of solids is kept constant through the simulation. In the mid-section of the riser, reducing the restitution coefficient had no noticeable effect on solids holdup. Altogether, simply reducing the restitution coefficient does not have a major effect on the vertical pressure gradient profiles, especially since the major discrepancies between experimental and computed data are observed at the mid-section of the riser (see Figure 5).

Effect of particle-wall friction

In the hydrodynamic model presented in Table 1, the Johnson and Jackson[26] partial-slip boundary condition is used for the solids phase. This wall boundary condition represents the frictional contact between particles and wall boundaries (particle-wall friction) through a specularity coefficient (ϕ). In accordance with an earlier study by Benyahia et al.,[15] which examined the effects of model parameters on core-annulus flow structure, a low value of ϕ (10^{-4}) was employed throughout this study. In this section, however, the effect of increasing the value of ϕ on the vertical profiles of solids hold-up and pressure gradient is examined. Note that the earlier study by Benyahia et al.[15] only examined periodic systems with a prescribed pressure drop, so no vertical profiles of flow variables were obtained. However, Benyahia et al.[15] found that clusters of particles tend to form slightly away from walls as ϕ is increased. As clusters tend to form away from walls, the gas will need to lift an increasing amount of solids, and the pressure gradient should increase. Therefore, higher friction between the particles and wall boundaries is anticipated to increase the pressure drop along the height of the riser. This hypothesis is investigated by conducting two simulations with increasing values of ϕ of 0.01 and 0.1 while keeping all other physical properties the same, as indicated in Table 2.

Figure 8 presents the effect of increasing the specularity coefficient on both the void fraction and pressure gradient profiles along the height of the riser for the EMMS model. As ϕ increases from 10^{-4} to 10^{-2}, the predicted pressure gradient profile (Figure 8b) increases significantly in the mid-section of the riser even though only a small increase in the solids hold-up (Figure 8a) is observed in this flow region. As ϕ is increased further to a value of 0.1, the pressure gradient profile overpredicts the experimental data in the mid-section of the riser (Figure 8b) while the solids hold-up decreases at the bottom region and increases at the mid-section of the riser (Figure 8a). Accordingly, more solids are transported along the height of the riser as the value of specularity coefficient is increased. Also, a comparison of Figures 8a,b shows that a

better agreement is obtained between the predicted values of the void fraction and pressure gradient profiles as the value of ϕ is increased. Collectively, these observations verify the earlier hypothesis that as ϕ is increased more solids clusters are forming away from walls and are lifted by the carrier gas, thus increasing the pressure gradient. Also worth noting is that the clusters forming away from walls were unstable and caused large fluctuations in pressure gradient profiles. This behavior is clearly noticeable for the largest value of ϕ used in this study. By using a longer time-averaging period, which was required for $\phi = 0.1$, these oscillations in pressure gradient are minimized. In summary, even with large values of specularity coefficient, the simulation predictions still do not reflect the experimentally-measured behavior of the gas-solids flow in this fluidized bed. Regardless, high values of particle-wall friction may be used with rough walls, which are sometimes intentionally designed to push solids away from wall regions (see for example, Jasti and Higgs[31]), whereas relatively low values of ϕ should be adopted with smooth walls, which are commonly used in experimental fluidized beds.

Effect of polydispersity

In this section the FCC particles are modeled as a polydisperse powder, i.e., having a particle size distribution (PSD), with three solids species as described previously (see Table 3). Using a single effective particle size (or monodisperse) to model FCC particles is common practice in the fluidization literature, such as in the work of Yang et al.,[28] Chalermsinsuwan et al.,[32,33] and Benyahia.[9] Bidisperse and polydisperse powders are less commonly considered in the literature due to additional complication in the granular kinetic theory model, increased computational requirements, etc. Two studies conducted at the University of Telmark (Norway) can be cited as examples of fluidization using a bidisperse[34] and polydisperse[35] powders. These authors and others have shown large segregation of particles due to their size distribution along the height of fluidized beds. Thus, two simulations that include a particle size distribution of the FCC powder are conducted in this section. One simulation is conducted with the standard homogeneous Wen-Yu drag law, and the second simulation uses the EMMS model (see Table 1).

Figure 9 presents the vertical profiles of void fraction deduced from the pressure gradient corresponding to the polydisperse case for the homogeneous Wen-Yu drag correlation and for the EMMS drag model, which accounts for the heterogeneous clusters of particles. These profiles are also compared with the monodisperse case for both drag models and the experimental data. The results obtained for the polydisperse case with the Wen-Yu drag are very similar to those of the monodisperse case using the same drag model. This comparison clearly shows that subgrid corrections to the Wen-Yu drag due to heterogeneous structures are necessary for polydisperse systems. In addition, the pressure gradient profile for the polydisperse case with the EMMS model is also similar to the monodisperse case using the same drag model. However, some differences are noticeable at the top and bottom region of the riser where the polydisperse case predicts slightly smaller and larger values of the pressure gradient, respectively. These slight differences between the mono- and poly-disperse predictions correspond to differences in the solids hold-up as demonstrated next.

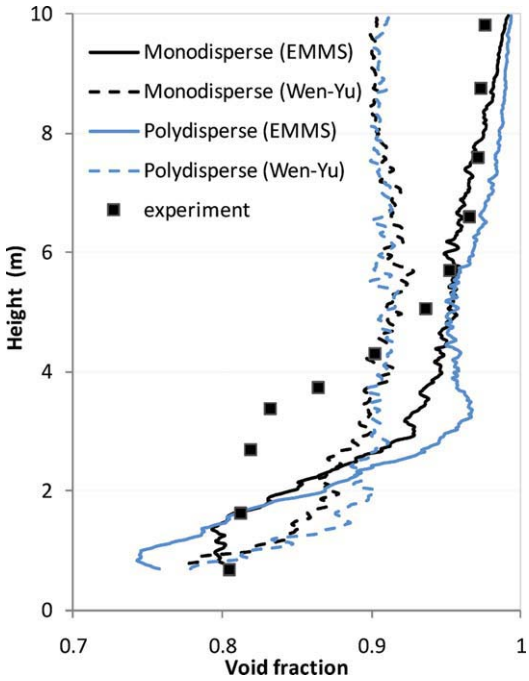

Figure 9. Effect of particle size distribution (using three solids species) on time-averaged void fraction vertical profiles (deduced from the computed pressure gradient) obtained with EMMS and homogeneous Wen-Yu drag correlations.

[Color figure can be viewed in the online issue, which is available at wileyonlinelibrary.com.]

The total solids hold-up for monodisperse and polydisperse cases along the height of the riser is shown in Figure 10 for the EMMS model. Also shown is the hold-up of the individual solids species in the polydisperse case. The total solids hold-up profiles are scaled with the total concentration of solids while the individual species solids hold-up are scaled with the averaged solids concentration of the respective individual species (values indicated in the figure). This scaling is necessary to clearly show the segregation of solids species due to size differences. Accounting for the polydisperse nature of FCC particles results in a larger total solids concentration at the bottom section of the riser and a smaller total solids hold-up at the top section as compared to the monodisperse case. As mentioned earlier, this behavior has a direct effect on the pressure gradient, which shows the same trend (see Figure 9). The profile of the total solids hold-up for the polydisperse case almost exactly follows the individual profile for the medium-size solids species (noted as dp_{60} in the figure) but is significantly different from the profile for the monodisperse case. Therefore, accounting for the polydisperse nature of FCC particles is necessary to accurately predict their vertical segregation due to gravity. This vertical segregation of particles due to size in a circulating fluidized bed has been noted previously by Mathiesen et al.,[35] who found large particles preferentially concentrate at the bottom section of the riser. The same behavior is computed in this study, albeit using a different polydisperse kinetic theory, which indicates higher concentrations of the large particle type at the bottom section of the riser and higher concentrations of the small particles at the top. At the

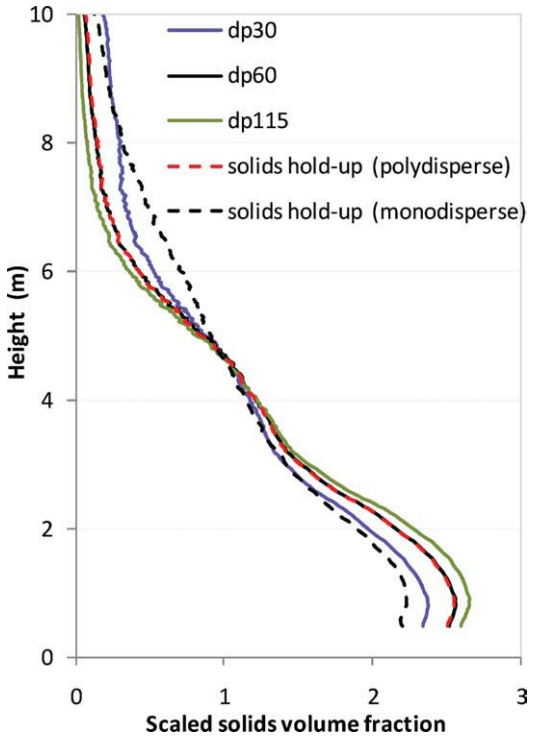

Figure 10. Total solids hold-up (discontinuous lines) and individual solids species hold-up (continuous lines) showing particle segregation by size along the vertical riser for the EMMS case.

Note that the plot of total solids hold-up for polydisperse case (discontinuous red line) is aligned with that of dp_{60} (continuous black line) and is difficult to distinguish. Solids hold-up is obtained by averaging the solids volume fraction along the horizontal direction at each vertical position. Computed solids volume fractions were scaled using domain-averaged volume fractions with the following values: 1.59% for d_{p30}; 6.35% for d_{p60}; 2.64% for d_{p115}; 10.58% for total solids hold-up. [Color figure can be viewed in the online issue, which is available at wiley onlinelibrary.com.]

midsection of the riser, similar values of total solids hold-up are obtained for both poly- and mono-disperse cases, meaning that the under-predicted values of pressure gradient in the midsection of the riser (shown in Figure 9) will not be correctly predicted for either case. One aspect worth mentioning of the polydisperse nature of powders is the fact that large particles can be transported to the top of the riser even when the terminal velocity of the large (heavy) particles is less than the superficial velocity of the carrying gas. These particles can be carried throughout the riser due to collisions with smaller particles (see for example the study of Nouyrigat et al.[36]). This behavior indicates that the transport of polydisperse particles in a circulating fluidized bed is affected not only by the gas-solids drag but also by collisions between unlike particles. Such behavior should be taken into account in the underlying kinetic theory for continuum modeling.

Summary

A computational study of the flow of air and FCC particles (Geldart group A powder) in a 2D circulating fluidized bed was conducted, and results demonstrate the need for subgrid scale modeling that will account for the formation of small clusters of particles such as have been observed experimentally. The use of the current EMMS drag model is proven to be both accurate and necessary for the prediction of the averaged solids mass and the pressure profile along the fully-developed flow region of the riser. The standard Wen-Yu drag model essentially predicts a homogeneous flow where the bed of particles is transported along the height of the riser. On the other hand, the inclusion of the EMMS drag in the hydrodynamic model prompts the formation of heterogeneous flow structures that limit the circulation of particles and corresponds to a more accurate prediction of the circulation rate of solids. This study also reveals the need to employ subgrid drag models when simulating the fluidization of polydisperse powders.

The effect of particle-particle friction was considered in this study by assuming slightly frictional particles and reducing the restitution coefficient during binary collisions as derived by Jenkins and Zhang.[30] As the restitution coefficient was decreased, segregation of particles to the bottom of the riser was observed to increase, but the impact on the pressure gradient profile was minor. The effect of increasing particle-wall friction on the vertical profiles in both solids segregation and pressure gradient was more noticeable. In particular, denser flow regions with increased pressure gradients were observed in the midsection of the riser as the specularity coefficient was increased. However, an intermediate value of this coefficient seems to better capture the experimentally measured pressure gradient profile. Other effects that can influence the model predictions include accounting for the 3D geometry of the entire circulating fluidized loop as well as accounting for the particle size distribution of FCC powder used experimentally. The study of these effects is left for future research.

Acknowledgments

The author acknowledges the help of Wei Wang (IPE, Chinese Academy of Sciences, Beijing) for sharing useful information and for writing the paragraph on the EMMS model in the introduction section. The author also appreciates useful discussions with Janine Galvin (NETL, Albany) and her many valuable comments on this work.

Notation

A_e, B_e, C_e = coefficients depending on void fraction in the EMMS drag model
C_D = gas-solids drag coefficient
d_p = particle diameter
e, e_w = particle-particle and particle-wall restitution coefficients
Fr, r, s = constants in frictional model,[23] equal to 0.5 dynes/cm^2, 2 and 5, respectively
$\mathbf{g}$ = acceleration of gravity
g_0 = radial distribution function at contact
H_d = EMMS-model correction factor to the Wen-Yu drag correlation
$\mathbf{I}$ = identity tensor
J_s = granular energy dissipation due to inelastic collisions
l_{mix} = constant gas-phase turbulent length scale
n = coefficient in the frictional model
$\mathbf{n}$ = unit vector normal to wall surface
P = pressure
$\mathbf{q}$ = flux of granular energy
Re = Reynolds number based on particle diameter
$\mathbf{S}_m$ = strain-rate tensor
t = time
$\mathbf{V}_m$ = velocity vector of phase m

Greek letters

α = constant in solids viscosity model,[26] equal to 1.6
β = gas-solids friction coefficient
δ, δ_w = angle of internal friction and wall friction of about $\pi/6$ and $\pi/10$, respectively
ε_m = phase-m volume fraction
ϕ = specularity coefficient used in wall boundary condition
η = constant depending on particle restitution coefficient equal to $(1+e)/2$
κ = solids phase dilute granular conductivity
κ^* = granular conductivity with effect of interstitial fluid
κ_s = conductivity of solids granular energy
μ = solids phase dilute granular viscosity
μ^* = granular viscosity with effect of interstitial fluid
μ_b = bulk viscosity of the solids phase
μ_m = dynamic viscosity of phase m
Π_Θ = production and dissipation of granular energy due to solids-fluid interaction
Θ_s = granular temperature
ρ_m = material density of phase m
τ = stress tensor

Indices

c = critical
f = frictional
g, s = gas and solids phases
k = kinetic-collisional
m = indices for the phases
max = maximum packing
min = minimum frictional solids fraction ($\varepsilon_s^{min} = 0.5$)
sl = particle-wall slip
w = wall

Literature Cited

1. Feng ZG, Michaelides EE. Heat transfer in particulate flows with direct numerical simulation (DNS). *Int J Heat Mass Trans*. 2009; 52:777–786.
2. Zhu HP, Zhou ZY, Yang RY, Yu AB. Discrete particle simulation of particulate systems: a review of major applications and findings. *Chem Eng Sci*. 2008;63:5728–5770.
3. Sanders RS, Schaan J, Hughes R, Shook C. Performance of sand slurry pipelines in the oil sands industry. *Can J Chem Eng*. 2004;82:850–857.
4. Jackson R. *The Dynamics of Fluidized Particles*. New York: Cambridge University Press, 2000.
5. Gidaspow D. *Multiphase Flow and Fluidization: Continuum and Kinetic Theory Description*. San Diego: Academic Press, 1994.
6. Bouillard JX, Lyczkowski RW, Gidaspow D. Porosity distributions in a fluidized bed with an immersed obstacle. *AIChE J*. 1989;35:908–922.
7. Wang J, van der Hoef MA, Kuipers JAM. Why the two-fluid model fails to predict the bed expansion characteristics of Geldart A particles in gas-fluidized beds: a tentative answer. *Chem Eng Sci*. 2009;64: 622–625.
8. Agrawal K, Loezos PN, Syamlal M, Sundaresan S. The role of meso-scale structures in rapid gas-solid flows. *J Fluid Mech*. 2001; 45:151–185.
9. Benyahia S. On the effect of subgrid drag closures. *Ind Eng Chem Res*. 2010;49:5112–5131.
10. Li J, Kwauk M. *Particle-Fluid Two-Phase Flow: the Energy-Minimization Multi-Scale Method; Metallurgy*. Beijing: Industry Press, 1994.
11. Wang W, Li J. Simulation of gas-solid two-phase flow by a multi-scale CFD approach—extension of the EMMS model to the sub-grid level. *Chem Eng Sci*. 2007;62:208–231.
12. Lu B, Wang W, Li J. Searching for a mesh-independent sub grid model for CFD simulation of gas–solid riser flows. *Chem Eng Sci*. 2009;64:3437–3447.
13. Kunii D, Levenspiel O. *Fluidization Engineering*. Boston: Butterworth-Heinemann, 1991.
14. Pope S. *Turbulent Flows*. New York: Cambridge University Press, 2000.
15. Benyahia S, Syamlal M, O'Brien TJ. Study of the ability of multiphase continuum models to predict core-annulus flow. *AIChE J*. 2007;53:2549–2568.
16. Lun CKK, Savage SB, Jeffrey DJ, Chepurniy N. Kinetic theories for granular flow—Inelastic particles in couette-flow and slightly inelastic particles in a general flowfield. *J Fluid Mech*. 1984;140:223–256.
17. Balzer G, Simonin O, Boelle A, Lavieville J. A unifying modeling approach for the numerical prediction of dilute and dense gas-solid two phase flow. Presented at the Preprints of *5th International Conference on Circulating Fluidized Beds*, Beijing, China, May 28–31, 1996.
18. Lun CKK, Savage SB. Kinetic theory for inertial flows of dilute turbulent gas-solids mixtures. Poeschel T, Brilliantov N, editors. *Granular Gas Dynamics*. Berlin: Springer-Verlag, 2003:267–289.
19. Iddir H, Arastoopour H. Modeling of multitype particle flow using the kinetic theory approach. *AIChE J*. 2005;51:1620–1632.
20. Benyahia, S. Verification and validation study of some polydisperse kinetic theories. *Chem Eng Sci*. 2008;63:5672–5680.
21. Iddir H. Modeling of the multiphase mixture of particles using the kinetic theory approach. PhD thesis, Illinois Institute of Technology, Chicago, IL, 2004.
22. Galvin JE. On the hydrodynamic description of binary mixtures of rapid granular flows and gas-fluidized beds. PhD thesis, University of Colorado, Boulder, CO, 2007.
23. Srivastava A, Sundaresan S. Analysis of a frictional-kinetic model for gas-particle flow. *Powder Tech*. 2003;129:72–85.
24. Benyahia S. Validation study of two continuum granular frictional flow theories. *Ind Eng Chem Res*. 2008;47:8926–8932.
25. Passalacqua A, Marmo LA. Critical comparison of frictional stress models applied to the simulation of bubbling fluidized beds. *Chem Eng Sci*. 2009;160:2795–2806.
26. Johnson PC, Jackson R. Frictional-collisional constitutive relations for granular materials, with application to plane shearing. *J Fluid Mech*. 1987;176:67–93.
27. Cocco R, Shaffer F, Hays R, Reddy Karri SB, Knowlton T. Particle clusters in and above fluidized beds. *Powder Technol*. 2010;203:3–11.
28. Yang N, Wang W, Ge W, Wang L, Li J. Simulation of heterogeneous structure in a circulating fluidized-bed riser by combining the two-fluid model with the EMMS approach. *Ind Eng Chem Res*. 2004;43:5548–5561.
29. Syamlal M. MFIX Documentation: numerical Technique: EG&G technical report, DE-AC21–95MC31346. 1998. Available at https://mfix.netl.doe.gov/documentation/numerics.pdf.
30. Jenkins JT, Zhang C. Kinetic theory for identical, frictional, nearly elastic spheres. *Phys Fluids*. 2002;14:1228–1235.
31. Jasti V, Higgs CF. Experimental study of granular flows in a rough annular shear cell. *Phys Rev E*. 2008;78:041306.
32. Chalermsinsuwan B, Piumsomboon B, Gidaspow D. Kinetic theory based computation of PSRI riser: part I-Estimate of mass transfer coefficient. *Chem Eng Sci*. 2009;64:1195–1211.
33. Chalermsinsuwan B, Piumsomboon B, Gidaspow D. Kinetic theory based computation of PSRI riser: part II-Computation of mass transfer coefficient with chemical reaction. *Chem Eng Sci*. 2009;64:1212–1222.
34. Mathiesen V, Solberg T, Arastoopour H, Hjertager BH. Experimental and computational study of multiphase gas/particle flow in a CFB riser. *AIChE J*. 1999;45:2503–2518.
35. Mathiesen V, Solberg T, Hjertager BH. Predictions of gas/particle flow with an Eulerian model including a realistic particle size distribution. *Powder Technol*. 2000;112:34–45.
36. Nouyrigat N, Ansart R, Neau H, Simonin O. A numerical study of fluidization behavior of bidispersed gas-solid flow using an Eulerian multifluid modeling approach. In: *Proceedings of the Les Rencontres Scientifiques de l'IFP* (1st International Conference on Chemical Looping), Lyon, France, March 17–19, 2010.

Manuscript received Sep. 29, 2010, and revision received Jan. 6, 2011.